Int. J. Solids Structures Vol. 15, pp. 643–658

0020-7683/79/0801-0643/$02.00/0

PLASTIC DEFORMATION AND STABILITY OF PIPES EXPOSED TO EXTERNAL COUPLES

PIROL TUGCU and J. SCHROEDER

Department of Civil Engineering, University of Waterloo, Ontario, Canada, N2L 3G1

(*Received* 1 *November* 1978; *in revised form* 27 *December* 1978)

Abstract—Buckling couples are determined from theoretical couple-displacement curves obtained by a plastic solution in terms of three-dimensional stress and strain satisfying end conditions. The plastic deformation is analyzed by describing the material behavior as rigid, hardening-plastic and by using the virtual work method for large nonlinear displacements. Deformation theory is employed to account for the dependency of stress on strain and hardening is considered to be linear, i.e. a constant modulus of plasticity is used. The theoretical results show good agreement with data of tests conducted by the authors on pipes.

The work indicates that plastic buckling loads can be predicted accurately in analogy with elastic stability analysis, i.e. by accounting for changes in shape only using a linear stress–strain relationship for the rigid-plastic material in conjunction with nonlinear strain-displacement relationships.

NOMENCLATURE

D and r_m	mean diameter and mean radius, respectively of plane pipes
T	thickness of pipe
l	length of plane pipe
σ_Y	average experimental yield strength of plane pipe of tee in tension
C_E	stable experimental limit couple of plane pipe
BC_E	experimental, plastic buckling couple of plane pipe
FC_E	experimental couple at first yield of a plane pipe
σ, ϵ	uniaxial stress, strain respectively
σ_Y	yield strength in tension
E_0	modulus of plasticity
$E_u, \bar{E}_u$	strain energy, complementary strain energy per unit volume for uniaxial condition
x, y, z	Cartesian coordinates
r, ϕ, z	general cylindrical coordinates
$\sigma_{zz}, \sigma_{\phi\phi}, \sigma_{rr}$ $\sigma_{rz}, \sigma_{r\phi}, \sigma_{\phi z}$	stress in cylindrical coordinates
$\epsilon_{zz}, \epsilon_{\phi\phi}, \epsilon_{rr}$ $\epsilon_{rz}, \epsilon_{r\phi}, \epsilon_{\phi z}$	strain in cylindrical coordinates
$s_{zz}, s_{\phi\phi}, s_{rr}$ $s_{rz}, s_{r\phi}, s_{\phi z}$	deviatoric stress in cylindrical coordinates
s_e, ϵ_e	equivalent or effective stress, strain
$E, \bar{E}$	strain energy, complementary strain energy per unit volume
δU	virtual change in total strain energy
δW	virtual work
V	undeformed volume of pipe
u, v, w	displacements along r, ϕ, z-direction
A_k, C_n	undetermined coefficients
u, j, k, m, n, p, q	summation indices
r^*	radius of deformed cross section of pipe
x^*	projection of r^* onto x-axis
$\bar{\sigma}_Y$	series expansion for σ_Y
BM	bending moment of pipe
M	moment of applied couple at end
R_o, R_i	outer and inner radius of plane pipe
S_{ij}	integrated coefficients of $\bar{\sigma}_Y$
BC_T	theoretical plastic buckling couple of plane pipe
BC_T^*	adjusted BC_T
R_m	mean radius of plane pipe used in appendix.

INTRODUCTION

A number of papers have dealt with elastic and/or plastic deformation and consequent buckling of pipes under bending. An elastic buckling solution was attempted in [1] by using a modified Donnell large deflection theory, i.e. a modified membrane shell theory, and by accounting for a change in shape of the cross section in the axial direction. Buckling was attributed to ovaling of the cross section and was predicted by setting the second variation of the potential energy to

zero. In [2] a number of pipes were deformed plastically under pipe-whip loading and a very approximate analysis of the results was attempted, using a simple moment-curvature relationship and a power law for the elastic–plastic stress–strain relationship where strain-hardening is represented by a power function of strain. A flattening of the cross section was not considered and the buckling moment was found by setting the derivative of the bending moment with respect to the slope of the longitudinal axis of the pipe to zero. A change in shape of the cross section was considered in a stable plastic solution of bending of thin-walled tubes under the assumption that this change was constant over the length of the pipe[3], i.e. without accounting for a variation in this change in the longitudinal direction of the tube. Shear strain and stresses were disregarded and the results were expressed by a moment-curvature relationship, based on a linear strain-displacement relationship and on a deformation theory type stress–strain law. Elastic–plastic stress–strain relationships were the same as in [2]. The same author proceeds in [4] to recover a buckling solution by equating the change in energy during buckling to the work done by the bending moment on buckling, i.e. by using a Timoshenko-type approach to this problem. Pre- and post-buckling behavior of infinitely long pipes exposed to longitudinal bending moments and external pressures were analysed in [5] by shell theory. The elastic–plastic stress–strain relationship was described using a power law and non-linear shell equations were employed to account for compatibility of deformation and equilibrium. A change in shape of the cross section was accounted for in the longitudinal and circumferential direction. Stability conditions were obtained by solving by trial and error a characteristic equation and selecting the smallest value of longitudinal stress corresponding to a certain hydrostatic pressure as the buckling stress. Post-buckling pressure-deflection curves were represented for constant longitudinal strain using numerical solutions of non-linear differential equations.

Using the principle of least work, elastic and plastic deformation was taken into account to find the ultimate moment of round tubing in [6]. End conditions and the effect of length were neglected, since a tube of unit length was analyzed, and shear on the middle surface of the shell was not considered. Length is one of the significant parameters in stability analysis. Because of these simplifications, the solution in [6] gives a lower bond to the experimental data.

This work appears then to be the first attempt to obtain a plastic solution for bent pipes using a fully three-dimensional stress and strain field, where variations in changes in cross sections are accounted for throughout the length of the pipe and boundary conditions are considered for all stresses and strains. In order to substantiate the solution experimentally, tests were conducted using the apparatus shown in Fig. 1. Test procedures are described in [7].

A DEFORMATION THEORY FOR RIGID PLASTIC LINEARLY HARDENING CYLINDRICAL SHELLS

In order to analyze the plastic deformation of pipes exposed to couples at the end, the following constitutive relationships are developed.

The experimental load–strain curve shown in Fig. 2 suggested that the material can be treated as rigid-plastic with linear hardening as indicated by results from a tensile test in Fig. 3 and the uniaxial stress–strain relationship can be approximated by

$$\sigma = \sigma_Y + E_0\epsilon \tag{1}$$

where σ and ϵ represent uniaxial stress and strain respectively and in analogy with elasticity E_0 is the modulus of plasticity. Equation (1) falls into the category of deformation theory since stress is directly related to strain and not to strain increments. The deformation theory is inaccurate when neutral loading occurs and/or the ratios of principle stress change significantly[8, 9]. Equation (1) and its generalization to multiaxial states of stress is maintained, since for the problem considered significant changes in the principle stress ratios are not expected and neutral loading is not taking place, but mainly since any more complicated plasticity theory renders the antisymmetric, plastic deformation due to bending of a pipe (representing a cylinderical shell) hopelessly complicated.

In using (1) and its generalization it is possible to employ the elastic analogue for the plastic analysis, which will be formulated under the following assumptions:

(i) The material obeys condition (1).
(ii) The changes in principle stress ratios are negligible.
(iii) Loads increase monotonically, i.e. no unloading or neutral loading takes place.
(iv) The displacements and rotations are large.

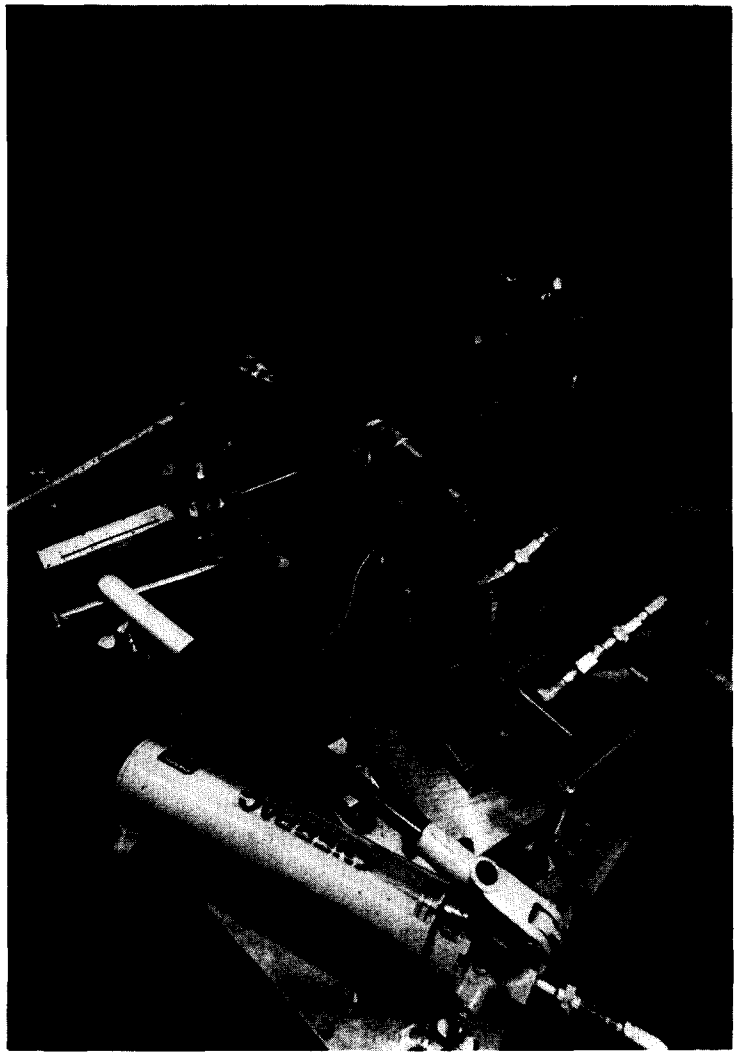

Fig. 1. Experimental set-up to bend pipes.

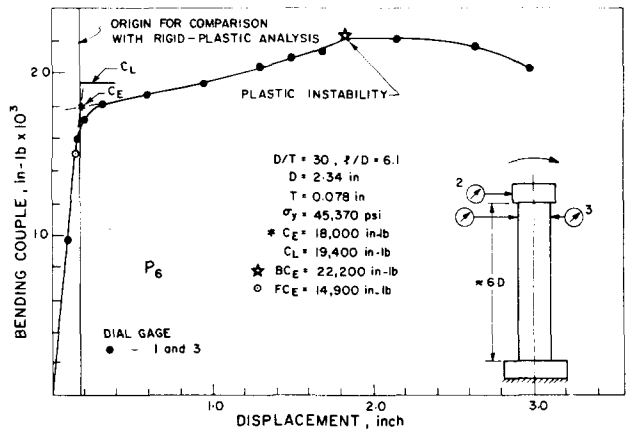

Fig. 2. Experimental load-displacement curve of pipe P_6.

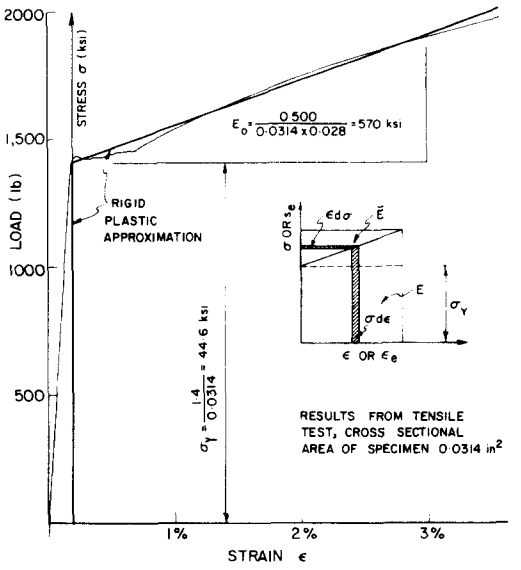

Fig. 3. Typical uniaxial load-strain curve for pipe material.

(v) Stains are negligible in comparison with unity and consequently the effect of changes in both orientation and magnitude of areas on stress are disregarded [8].

Considering the insert in Fig. 3 it can be seen that

$$\sigma\epsilon = \int_0^{\epsilon} \sigma \, d\epsilon + \int_{\sigma_Y}^{\sigma} \epsilon \, d\sigma. \tag{2}$$

Denoting

$$E_u = \int_u^{\epsilon} \sigma \, d\epsilon, \quad \bar{E}_u = \int_{\sigma_Y}^{\sigma} \epsilon \, d\sigma \tag{3}$$

it follows from a total arbitrary variation of (2) that

$$\left(\frac{\partial E_u}{\partial \epsilon} - \sigma\right) \delta\epsilon + \left(\frac{\partial \bar{E}_u}{\partial \sigma} - \epsilon\right) \delta\sigma = 0 \tag{4}$$

and

$$\sigma = \frac{\partial E_u}{\partial \epsilon}, \quad \epsilon = \frac{\partial \bar{E}_u}{\partial \sigma}. \tag{5}$$

The multiaxial state of stress (σ_{zz}, $\sigma_{\phi\phi}$, σ_{rr}, σ_{rz}, $\sigma_{r\phi}$, $\sigma_{\phi z}$) and strain (ϵ_{zz}, $\epsilon_{\phi\phi}$, ϵ_{rr}, ϵ_{rz}, $\epsilon_{r\phi}$, $\epsilon_{\phi z}$) shown for z, ϕ, r cylindrical coordinates in Fig. 4 has to be exposed to the plastic incompressibility condition

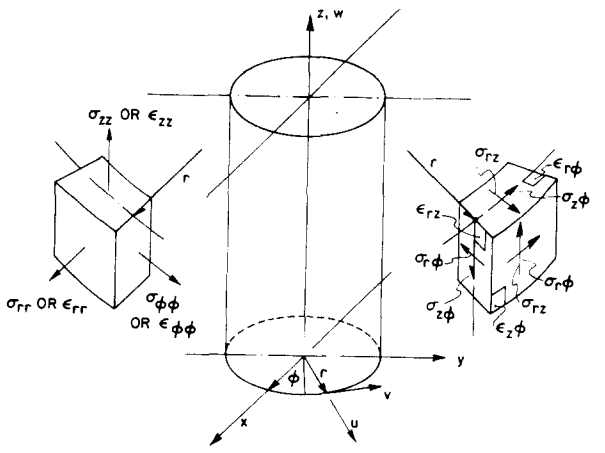

Fig. 4. Stress and strain components used in analysis.

$$\epsilon_{rr} + \epsilon_{\phi\phi} + \epsilon_{zz} = 0 \tag{6}$$

and will be restricted for shells by

$$\sigma_{rr} = 0. \tag{7}$$

Since in view of (6) plastic strain is independent of hydrostatic pressure; the plastic deformation is governed by deviatoric stress[8] which considering (7) can be expressed as

$$s_{zz} = \frac{2}{3}\left(\sigma_{zz} - \frac{1}{2}\sigma_{\phi\phi}\right), \quad s_{\phi\phi} = \frac{2}{3}\left(\sigma_{\phi\phi} - \frac{1}{2}\sigma_{zz}\right), \text{ etc.} \tag{8}$$

In order to generalize (1)–(5) $\sigma\epsilon$ in (2) may be replaced by

$$s_e\epsilon_e = s_{zz}\epsilon_{zz} + s_{\phi\phi}\epsilon_{\phi\phi} + \cdots, s_{z\phi}\epsilon_{z\phi} \tag{9}$$

where in view of (7) and (8)

$$s_e^2 = \sigma_{zz}^2 + \sigma_{\phi\phi}^2 - \sigma_{zz}\sigma_{\phi\phi} + 3(\sigma_{rz}^2 + \sigma_{r\phi}^2 + \sigma_{z\phi}^2) \tag{10}$$

ϵ_e is chosen to satisfy (9), i.e. in view of (6)

$$\epsilon_e^2 = \frac{4}{3}(\epsilon_{zz}^2 + \epsilon_{\phi\phi}^2 + \epsilon_{zz}\epsilon_{\phi\phi} + \epsilon_{rz}^2 + \epsilon_{r\phi}^2 + \epsilon_{z\phi}^2) \tag{11}$$

s_e and ϵ_e are so called equivalent or effective stress and strain respectively[8, 9].

In accordance with von Mises[10] the material undergoes first yield when

$$s_e = \sigma_Y \tag{12}$$

and it will be assumed that for multiaxial states of stress and strain the relationship (1) is valid in the form

$$s_e = \sigma_Y + E_0\epsilon_e \quad \text{or} \quad \epsilon_e = \frac{s_e - \sigma_Y}{E_0}. \tag{13}$$

Thus, multiaxial results can be correlated with uniaxial results using (13). This means, for example that multiaxial results expressed in terms of s_e and ϵ_e should follow the uniaxial σ vs ϵ curve shown in Fig. 3. Replacing σ and ϵ by s_e and ϵ_e respectively in (3), it follows considering (13) that for the multiaxial state of stress

$$E = \int_0^{\epsilon_0} s_e \, d\epsilon_e = \sigma_Y\epsilon_e + \frac{1}{2}E_0\epsilon_e^2, \quad \bar{E} = \int_{\sigma_Y}^{s_e} \epsilon_e \, ds_e = \frac{1}{2}E_0(s_e - \sigma_Y)^2. \tag{14}$$

Using the elastic analogy, E is the strain energy or dissipative potential per unit volume and $\bar{E}$ is the complementary of it as shown in the insert of Fig. 3.

The multiaxial stress–strain relationships can be found in analogy with (5). Thus, for example

$$s_{zz} = \frac{\partial E}{\partial \epsilon_e}\frac{\partial \epsilon_e}{\partial \epsilon_{zz}} = \frac{2}{3}\left(\frac{\sigma_Y}{\epsilon_e} + E_0\right)\epsilon_{zz} \tag{15}$$

and considering the same expression for $s_{\phi\phi}$ and (8)

$$\sigma_{zz} = \frac{2}{3}\left(\frac{\sigma_Y}{\epsilon_e} + E_0\right)(2\epsilon_{zz} + \epsilon_{\phi\phi}), \text{ etc.} \tag{16}$$

THE METHOD OF VIRTUAL WORK FOR LARGE DISPLACEMENTS

The method simply postulates[11] that the change in total strain energy due to virtual displacements equals the work done by the applied forces on the virtual displacement. Thus, using δ for virtual changes as well as for variations

$$\delta U = \delta W \tag{17}$$

where in view of (14)

$$\delta U = \int_V \delta E \, \mathrm{d}V \tag{18}$$

and δW is the virtual work. Considering (14) it follows that

$$\delta E = \frac{\partial E}{\partial \epsilon_{zz}} \delta \epsilon_{zz} + \frac{\partial E}{\partial \epsilon_{\phi\phi}} \delta \epsilon_{\phi\phi} + \cdots \tag{19}$$

since E depends on strain only. In view of (15) this can be rewritten as

$$\delta E = s_{zz}\delta\epsilon_{zz} + s_{\phi\phi}\delta\epsilon_{\phi\phi} + \cdots = \sigma_{zz}\delta\epsilon_{zz} + \sigma_{\phi\phi}\delta\epsilon_{\phi\phi} + \cdots. \tag{20}$$

The last equality is a consequence of (6) and (8). Thus δU in (17) can be expressed as

$$\delta U = \int_V (\sigma_{zz}\delta\epsilon_{zz} + \sigma_{\phi\phi}\delta\epsilon_{\phi\phi} + \cdots, \sigma_{z\phi}\delta\epsilon_{z\phi}) \, \mathrm{d}V. \tag{21}$$

The arbitrary variations of strain $\delta\epsilon_{zz}$, etc. can be expressed in terms of virtual displacements. Using u, v, w for displacements in the radial, tangential and axial direction as shwon in Fig. 4 the strain-large displacement relationships[11] can be expressed in cylindrical coordinates as

$$\epsilon_{zz} = \frac{\partial w}{\partial z} + \frac{1}{2}\left(\frac{\partial u}{\partial z}\right)^2 + \frac{1}{2}\left(\frac{\partial v}{\partial z}\right)^2 + \frac{1}{2}\left(\frac{\partial w}{\partial z}\right)^2 \tag{22a}$$

$$\epsilon_{\phi\phi} = \frac{u}{r} + \frac{1}{r}\frac{\partial v}{\partial \phi} + \frac{1}{2r^2}\left(\frac{\partial u}{\partial \phi} - v\right)^2 + \frac{1}{2r^2}\left(u + \frac{\partial v}{\partial \phi}\right)^2 \tag{22b}$$

$$\epsilon_{rr} = \frac{\partial u}{\partial r} + \frac{1}{2}\left(\frac{\partial u}{\partial r}\right)^2 + \frac{1}{2}\left(\frac{\partial v}{\partial r}\right)^2 + \frac{1}{2}\left(\frac{\partial w}{\partial r}\right)^2 \tag{22c}$$

$$\epsilon_{rz} = \frac{1}{2}\left(\frac{\partial u}{\partial z} + \frac{\partial w}{\partial r}\right) + \frac{\partial w}{\partial z}\frac{\partial w}{\partial r} + \frac{\partial v}{\partial r}\frac{\partial v}{\partial z} + \frac{\partial u}{\partial r}\frac{\partial u}{\partial z} \tag{22d}$$

$$\epsilon_{r\phi} = \frac{1}{2}\left(\frac{\partial v}{\partial r} - \frac{v}{r} + \frac{1}{r}\frac{\partial u}{\partial \phi}\right) - \frac{1}{r}\left(\frac{\partial w}{\partial r}\frac{\partial w}{\partial \phi}\right) + \frac{1}{r}\left(\frac{\partial v}{\partial \phi}\frac{\partial v}{\partial r}\right) + \frac{u}{r}\frac{\partial v}{\partial r} + \frac{1}{r}\frac{\partial u}{\partial r}\frac{\partial u}{\partial \phi} - \frac{v}{r}\frac{\partial u}{\partial r} \tag{22e}$$

$$\epsilon_{z\phi} = \frac{1}{2}\left(\frac{\partial v}{\partial z} + \frac{1}{r}\frac{\partial w}{\partial \phi}\right) + \frac{1}{r}\frac{\partial w}{\partial z}\frac{\partial w}{\partial \phi} + \frac{1}{r}\frac{\partial v}{\partial z}\frac{\partial v}{\partial \phi} + \frac{1}{r}\frac{\partial u}{\partial z}\frac{\partial u}{\partial \phi} - \frac{v}{r}\frac{\partial u}{\partial z} + \frac{u}{r}\frac{\partial v}{\partial z}. \tag{22f}$$

It is shown in [11] that in expressing the $\delta\epsilon_{zz}$, $\epsilon_{\phi\phi}$, etc. in (19) in terms of δu, δv, δw using (22), eqn (21) yields the equilibrium condition for small strain but accounting for arbitrary rotation of infinitesimal volume elements.

Since in view of the first equation in (14) E depends on strain only and can be expressed in terms of displacement using (22), it is possible to rewrite (17) in view of (18) as:

$$\int_V \left(\frac{\partial E}{\partial u}\delta u + \frac{\partial E}{\partial v}\delta v + \frac{\partial E}{\partial w}\delta w\right) \mathrm{d}V = \delta W. \tag{23}$$

In this form the virtual work method yields three equations which permits one to solve for u, v and w and the stresses can be calculated using (16). This reduces the study of the equilibrium of a deformed body to the solution of (23) provided u, v and w satisfy the proper boundary conditions.

The virtual work solution (23) is very useful for the applications of numerical methods, where u, v, w nad consequently E and W are expressed in terms of infinite series and the undetermined coefficients of these series are found by taking arbitrary variations with respect to these coefficients. This method will be used to obtain an approximate solution for large plastic deformation of a plane pipe exposed to a couple at the end.

DISPLACEMENT FIELDS USED FOR THE SOLUTION

The solution is formulated by considering one half of the pipe shown in Fig. 5, which resembles the section of P_6 shown in Fig. 7, but without the dent due to local plastic deformation.

The displacement field was formulated with respect to the original position of the pipe in the following way: First the displacement u was constructed in the form of a series to permit the cross section to change shape and position as indicated in Fig. 6 and to satisfy the proper boundary conditions at the ends, i.e.

$$u = A_k\left(1-\cos\frac{k\pi z}{l}\right)\cos\phi - C_n\cos 2\phi\left(\cos\frac{2n\pi z}{l}+1\right)$$

$$\frac{\partial u}{\partial z} = 0 \quad \text{when} \quad z = 0 \tag{24}$$

$$u = 0, \frac{\partial u}{\partial z} = 0 \quad \text{when } z = \frac{l}{2}.$$

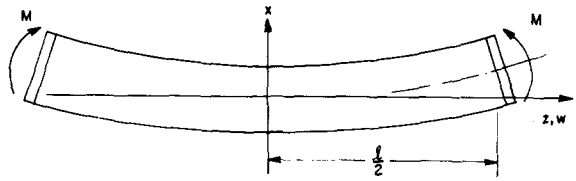

Fig. 5. Deformed, longitudinal shape of pipe used in analysis.

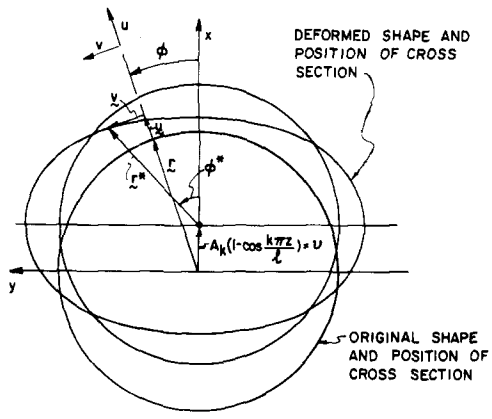

Fig. 6. Deformed, transverse normal section of pipe used in analysis.

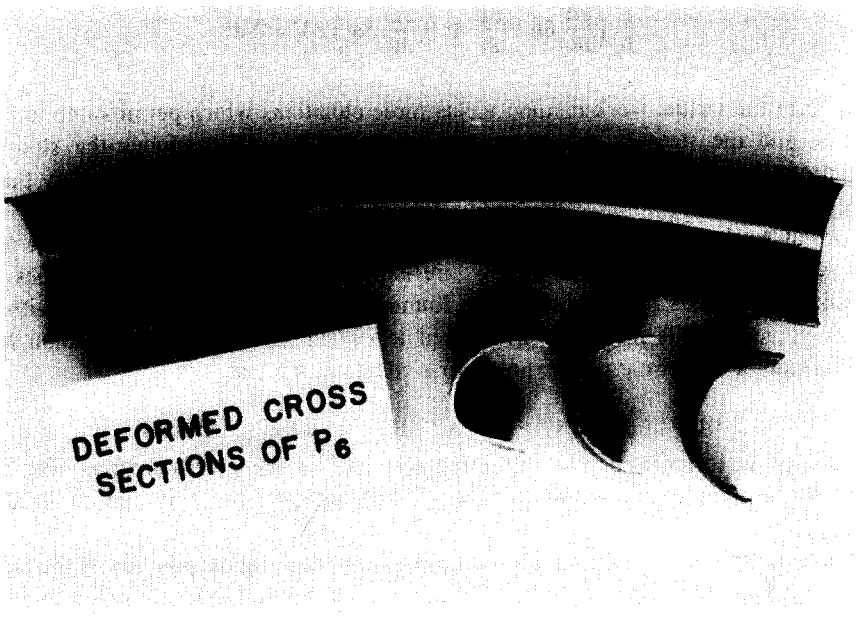

Fig. 7. Deformed cross sections of tested pipe P_6.

A_k and C_n are undertermined coefficients and summed over k and n, where $n = 1, 3, 5, \ldots$. The displacement v was selected such that for linear terms $\epsilon_{\phi\phi}$ is due to bending only and thus vanishes at the middle surface where $r = r_m$ and

$$\frac{1}{2}\left(\frac{\partial v}{\partial r} - \frac{v}{r} + \frac{1}{r}\frac{\partial u}{\partial \phi}\right) = 0 \quad \text{for any } r, \tag{25}$$

i.e. in view of (22e) the linear part of $\epsilon_{r\phi}$ is zero everywhere.

Thus

$$v = -A_k\left(1 - \cos\frac{k\pi z}{l}\right)\sin\phi + \frac{1}{2}C_n \sin 2\phi\left(\cos\frac{2n\pi z}{l} + 1\right)$$
$$-(r - r_m)\frac{3}{2r}C_n \sin 2\phi\left(\cos\frac{2\pi z}{l} + 1\right) \tag{26}$$

$$\frac{\partial v}{\partial z} = 0 \quad \text{when} \quad z = 0$$

$$v = 0, \frac{\partial v}{\partial z} = 0 \quad \text{when} \quad z = \frac{l}{2}.$$

And finally the displacement w was constructed such that for linear terms only the shear strain ϵ_{zr} vanishes, i.e. in view of (22d)

$$\frac{1}{2}\left(\frac{\partial u}{\partial z} + \frac{\partial w}{\partial r}\right) = 0 \quad \text{for any } r \tag{27}$$

and consequently

$$w = r\frac{\partial u}{\partial z} + F(\phi, z). \tag{28}$$

The function $F(\phi, z)$ was chosen to represent w in the form

$$w = r^*\frac{\partial u}{\partial z} + \cdots. \tag{29}$$

where r^* is the radius of the deformed cross section shown in Fig. 6 and accounts also for the shifting of the neutral axis. It follows from that figure that the vector

$$\mathbf{r}^* = \mathbf{r} + \mathbf{u} + \mathbf{v} - \boldsymbol{\nu}, \nu = A_k \left(1 - \cos \frac{k\pi z}{l}\right) \tag{30}$$

and that the projection of r^* onto the x-axis is

$$x^* = r^* \cos \phi^* = r \cos \phi + u \cos \phi - v \sin \phi - \nu. \tag{31}$$

Approximating

$$r^* \cos \phi \approx r^* \cos \phi^* \tag{32}$$

it follows from (29), (31), (24), (27) that

$$w = -A_k \left[r \cos \phi - C_n \left(\cos 2\phi \cos \phi + \frac{1}{2} \sin 2\phi \sin \phi \right) \left(\cos \frac{2n\pi z}{l} + 1 \right) \right] \frac{k\pi}{l} \sin \frac{k\pi z}{l}$$

$$-(r - r_m) \left(C_n \frac{2n\pi z}{l} \cos 2\phi \sin \frac{2n\pi z}{l} \right). \tag{33}$$

$w = 0$ when $z = 0$.

The term $(r - r_m)$ was chosen instead of r since it accounts as in shell theory for bending strain due to curvature changes of the middle surface of the shell and does not interfere with (27); r_m denotes the mean radius of plane pipes.

The boundary conditions satisfied in (24), (26), (33) are those of the pipes tested, i.e. they account for the reinforcements of the pipes at the ends as shown in Fig. 1.

The strain energy density E for the virtual work principle defined in (23) was chosen in form of the first equation in (14), i.e.

$$\delta U = \int_V \delta E \, \mathrm{d}V = \int_V \delta \left(\sigma_Y \epsilon_e + \frac{1}{2} E_0 \epsilon_e^2 \right) \mathrm{d}V = \delta W. \tag{34}$$

The solution of this equation is complicated by the first term of the integrant $\sigma_Y \epsilon_e$ representing the rectangular area of E shown in the insert of Fig. 3, since it involves the radical ϵ_e defined in (11) which complicates both integration and variation. Equation (34) was solved using some simplifications for ϵ_e and also for ϵ_e^2. Firstly the simplifying assumptions made for ϵ_e^2 were:

(a) The strain-displacement relationship for ϵ_{rr} in (22c) are disregarded in order to satisfy the more important incompressible condition (6). This should not cause a significant error since the term $\sigma_{rr} \delta \epsilon_{rr}$ in (21) vanishes because of (7).

(b) $$\epsilon_{rz} = \epsilon_{r\phi} = 0, \tag{35}$$

i.e. as u, v and w were chosen to render the linear terms of ϵ_{rz}, $\epsilon_{r\phi}$ zero, the nonlinear terms are neglected.

(c) Considering (24), (26), (22b),

$$\epsilon_{\phi\phi} = -\frac{r - r_m}{r^2} 3C_n \cos 2\phi \left(\cos \frac{2n\pi z}{l} + 1 \right) + \cdots.$$

Consequently, except for the nonlinear terms $\epsilon_{\phi\phi}$ vanishes on the middle surface. However in view of (22a) and (33) the linear term $\partial w / \partial z$ in ϵ_{zz} is not zero when $r = r_m$ and would cause a stress $\sigma_{\phi\phi}$ at the middle surface in view of (16). In order to insure that for the linear portion of the solution

$$\sigma_{\phi\phi} = 0 \quad \text{when} \quad r = r_m \tag{36}$$

it is necessary to choose

$$\epsilon_{\phi\phi} = -\frac{1}{2}\frac{\partial w}{\partial z}(r = r_m) + \frac{u}{r} + \frac{1}{r}\frac{\partial v}{\partial \phi} + \cdots. \tag{37}$$

Under assumptions (a)–(c) it follows in view of (11) that

$$\epsilon_e^2 = \frac{4}{3}(\epsilon_{zz}^2 + \epsilon_{\phi\phi}^2 + \epsilon_{zz}\epsilon_{\phi\phi} + \epsilon_{z\phi}^2). \tag{38}$$

This will be further approximated for the radical, i.e.

(d)
$$\epsilon_e = \frac{2}{\sqrt{3}}(\epsilon_{zz}^2 + \epsilon_{\phi\phi}^2 + \epsilon_{zz}\epsilon_{\phi\phi} + \epsilon_{z\phi}^2)^{1/2} \approx \epsilon_{zz} \tag{39}$$

for the term $\sigma_Y \epsilon_e$ appearing in (34). This last assumption is made to obtain a manageable solution. By rechecking ϵ_e after solutions were obtained the error did not exceed 10% which is mainly due to (37). It should be noted that a 10% error in (39) due to neglecting $\epsilon_{\phi\phi}^2$ and $\epsilon_{z\phi}^2$ causes a much larger error if the same terms are neglected in (38).

In view of the assumption shown in (39) it was necessary to express σ_Y as a double series such that terms in the linear portion of ϵ_{zz} did not drop out on integration. Thus, σ_Y was replaced by

$$\bar{\sigma}_Y = \sigma_Y \left(1.73 \cos\frac{\pi z}{l} - 1.1 \cos\frac{2\pi z}{l} + 0.46 \cos\frac{3\pi z}{l} - 0.1 \cos\frac{4\pi z}{l}\right)$$
$$\times \left(-\cos\phi + \frac{1}{3}\cos 3\phi\right)\frac{4}{\pi}. \tag{40}$$

E was calculated as indicated in (14) using the simplified expressions (38), (39) and condition (40). Strains were then expressed in (14) in terms of displacements u, v, w employing (22) and these displacements were rewritten using the series given in (24), (26) and (33). A variation of E in this form with respect to A_K and C_n resulted in a set of nonlinear equations of third order in A_K and C_n and a solution of these equations yielded three roots for each A_K and C_n. This made the determination of the minimum energy corresponding to each displacement close to impossible using a computer. Consequently, it was decided to maintain third order terms for A_K and C_n only in (14), (i.e. in view of (22) products of linear and of linear with nonlinear strain terms), which yielded a set of nonlinear, second order equations for A_K and C_n after variations. This procedure led to accurate predictions of experimental results.

The virtual work principle (34) was restricted by the condition that the bending moment BM equals the moment M of the applied couple at the end, i.e.

$$BM = \int x^* \sigma_{zz}\, dA = M \tag{41}$$

where σ_{zz} can be calculated in terms of u, v and w using (16) and (22). The restriction was imposed at three sections using the method of Lagrangian multipliers in connection with (34). The nonlinear, second order equations were solved using the computer program ZSYSTM. The nonlinear equations which were solved are given in the Appendix.

DISCUSSION OF RESULTS

Sections of three deformed pipes P_6, P_8 and P_7 are shown in Figs. 7, 9 and 11 respectively. A comparison of theoretical solutions with experimental results is made for these pipes in Figs. 8, 10 and 12, which show that the theoretical bending couple-displacement curves are above the corresponding experimental curves. This is partly due to the fact that the theoretical limit couple

$$C_L = 4Tr_m^2\sigma_Y \tag{42}$$

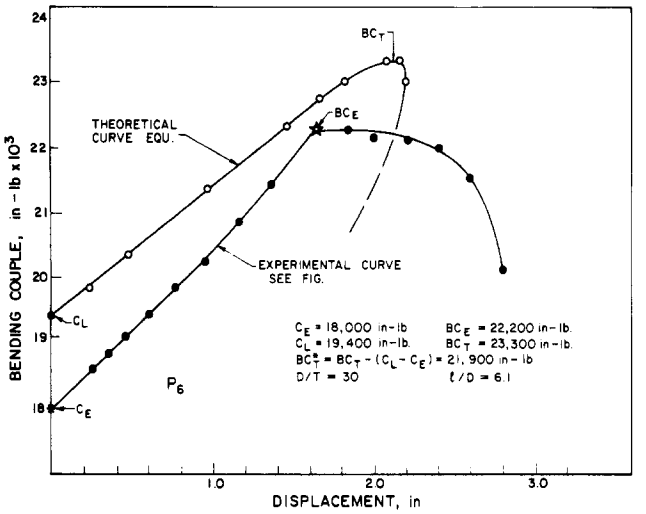

Fig. 8. Comparison of theoretical with experimental load-displacement curves of pipe P_6.

was used as the origin of the theoretical curves. C_L is, in general, about 10% higher than the experimental limit couple C_E[12]. This is also evident from Fig. 2. It can be seen that experimental and theoretical curves have about the same slope in Figs. 8, 10 and 12 and that the differences in the experimental and theoretical plastic buckling couples, i.e. the BC_E and BC_T, are 5, 12 and 17% of BC_E for P_6, P_8 and P_7 respectively. If a theoretical plastic buckling couple

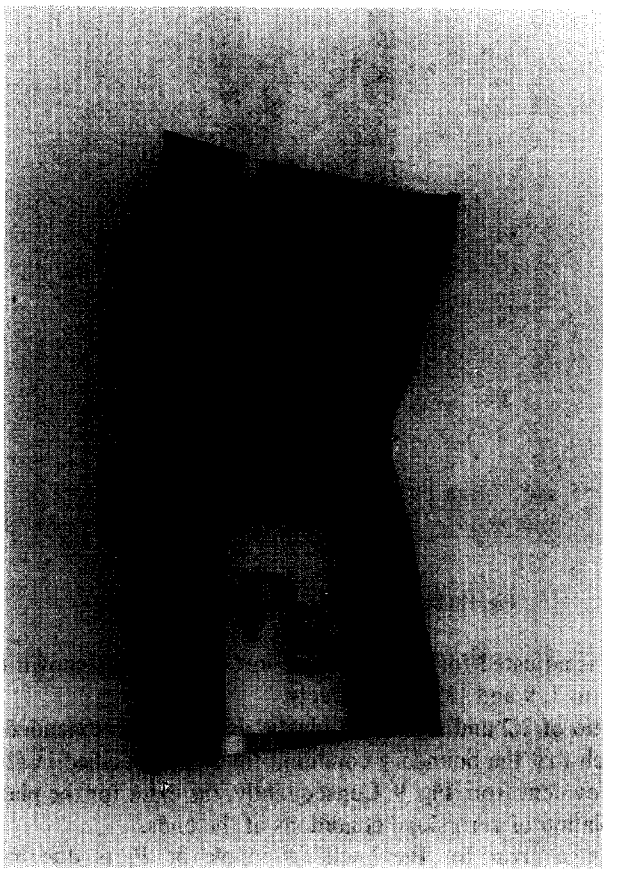

Fig. 9. Deformed cross section of tested pipe P_8.

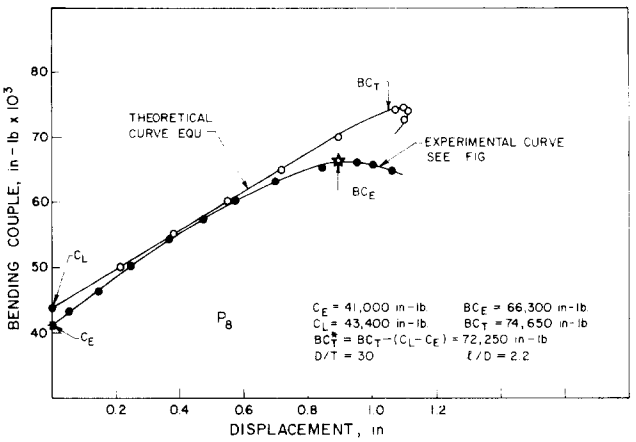

Fig. 10. Comparison of theoretical with experimental load-displacement curves for pipe P_8.

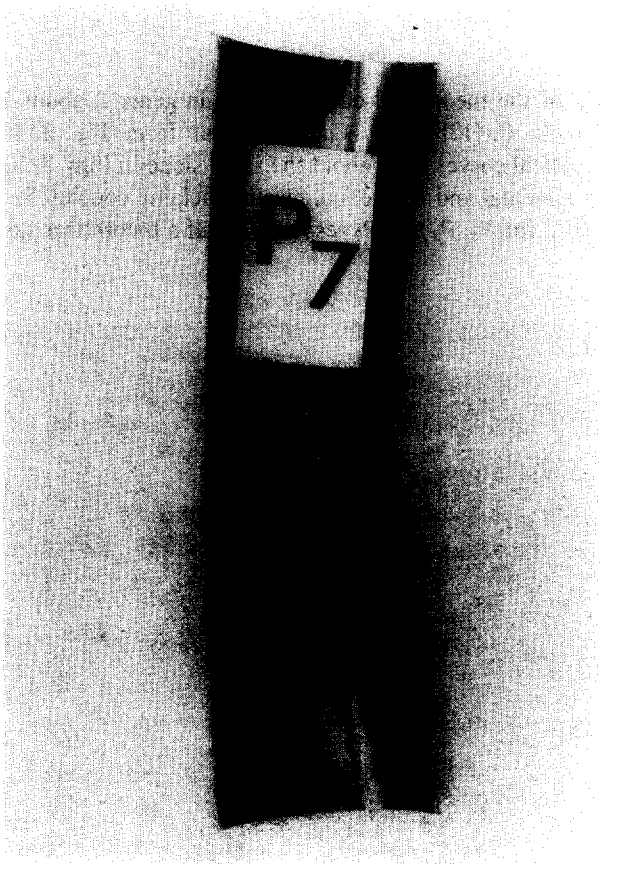

Fig. 11. Deformed cross section of tested pipe P_7.

BC_T^* is used, which is adjusted for the difference in C_E and C_L as shown in these figures, the above errors change to 1, 9 and 13% respectively.

P_8 had an l/D ratio of 2.2 and significant plastic deformations extended to the ends of this rather short pipe such that the boundary condition for slope specified in (24) for the ends was not satisfied. This is evident from Fig. 9. Consequently, the error for the plastic buckling couple of P_8 is due to a violation of zero slope conditions at the ends.

The high percentage error for the buckling couple of P_7 is due to significant elastic deformations, which are neglected in this analysis. P_7 had a diameter/thickness ratio of 50, whereas for P_6 and P_8 this ratio was 30. It is evident from Figs. 11 and 13 that the buckling of

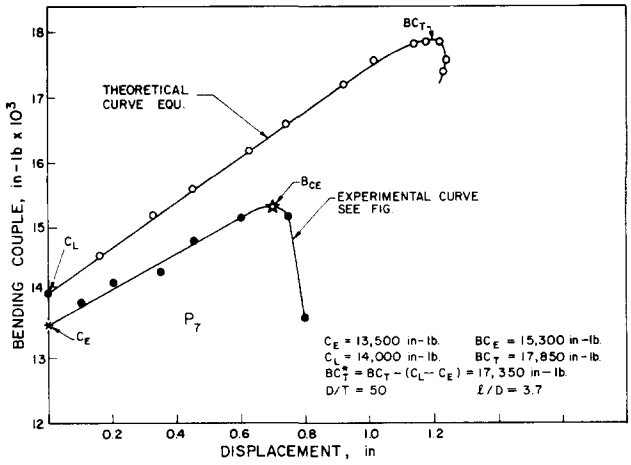

Fig. 12. Comparison of theoretical with experimental load-displacement curves for pipe P_7.

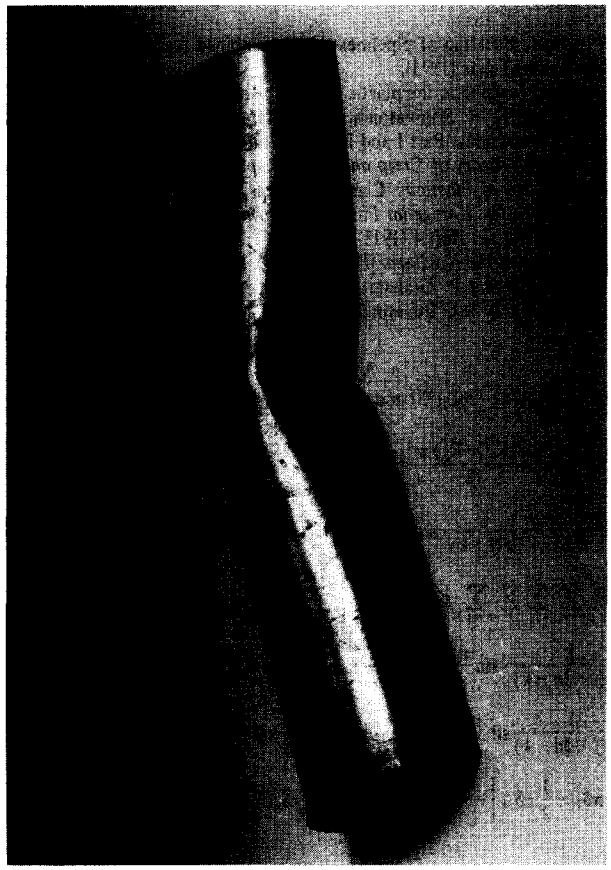

Fig. 13. Local elastic–plastic dent of pipe P_7.

P_7 was due to a local elastic–plastic snap-through rather than a plastic gross-deformation of shape evident in Figs. 7 and 9 for P_6 and P_8 respectively. For these two pipes the bending couple decreased gradually after buckling as indicated in Figs. 8 and 10 and the local dent visible in Figs. 7 and 9 occurred after plastic gross-deformations of shape. The elastic–plastic snap-through of P_7 is also evident in Fig. 12 for two reasons: the bending couple decreases rapidly after buckling and the experimental buckling couple BC_E occurs at a considerably smaller displacement than predicted theoretically. The behavior of P_6 and P_8 is quite different in this respect as can be seen in Figs. 8 and 10. All theoretical curves turn towards the moment axis after BC_T was reached and consequently do not predict post-buckling behavior correctly,

which is to be expected. It is also interesting to note, that because of this turn, a second couple exists which corresponds to the displacement due to BC_T. This duality of the solution is due to the mathematical nonlinearity of the equations. The second couple has no physical meaning as far as buckling is concerned since there is no perturbation in slope at that point.

The complexity of the strain energy indicates that a power law for the stress–strain relationship as used in [2–4] for a one dimensional approach renders a three dimensional solution hopelessly complicated because of integration anf variation. This is the main reason the rigid, linearly hardening description was used in this work and with success as indicated in Figs. 8 and 10.

Acknowledgement—This work was supported by the National Research Council of Canada Grant No. A-3817.

REFERENCES

1. J. C. Yao, Large deflection analysis of buckling of a cylinder under bending. *J. Appl. Mech. Trans. ASME* 708–714 (1962).
2. T. L. Gerber, Plastic deformation of piping due to pipe-whip loading. *Pres. ASME Meeting*, Miami (1974).
3. L. G. Afendik, Bending thin-walled tubes with considerable curvature beyond the elastic limit. *Prikladnaya Mekhanika* 4(6), 45–51 (1968).
4. L. G. Afendik, The stability of a circular cylindrical shell in bending beyond the elastic limit. *Prikladnaya Mekhanika* 6(9) 39–44 (1970).
5. T. G. Johns and alias, Inelastic buckling of pipelines under combined loads; Paper No. OTC 2209, *pres. 7th Annual Offshore Techn. Conf.* Houston, Texas (1975).
6. C. F. Ades, Bending strength of tubing in the plastic range. *J. Aero. Sci.* (1957).
7. J. Schroeder, J. Gartenberg and K. R. Srinivasaiah, Limit interaction and external couples and internal pressure for branch-pipe lateral and tee connections, Part I and II. *Proc. 2nd Int. Conf. Pressure Vessel Techn.* Texas (1973).
8. F. K. G. Odquist, *Mathematical Theory of Creep and Creep Rupture.* Clarendon Press, Oxford (1966).
9. R. Hill, *The Mathematical Theory of Plasticity.* Clarendon Press, Oxford (1950).
10. R. Von Mises, *Mechanik der Festen Körper im Plastich-Deformablem Zustand*, pp. 582–592. Göttinger Nachrichten, Mathematische-Physikalische Klasse, Heft 4 (1913).
11. V. V. Novozhilov, *Foundations of the Nonlinear Theory of Elasticity.* Graylock Press, New York (1953).
12. J. Schroeder, K. R. Srinivasaiah and P. Graham, Analysis of test data on branch connections exposed to internal pressure and/or external couples. W R C Bulletin 200 (1974).

APPENDIX

Considering (34), (14), (38)–(40), (24), (26), (33) and assumptions (a)–(d) it follows that:

$$
\begin{aligned}
U = \int E\,\mathrm{d}V = 4\Bigg\{ & -\frac{(R_o^3 - R_i^3)}{12}\frac{\pi^2}{l}\sum_{i=1,3}\sum_{j}\sum_{k} S_{ij}A_k k^2 \pi\delta_{1i}\left[\frac{1}{\pi(j-k)}\right. \\
& \left.\times \sin\frac{\pi(j-k)}{2} + \frac{1}{\pi(j+k)}\cdot\sin\frac{\pi(j+k)}{2}\right] \\
& + \frac{TR_m}{8}\sum_{i=1,3}\sum_{j}\sum_{k}\sum_{n=1,3} s_{ij}C_n A_k k^2 \frac{\pi^2}{l}\left[\frac{1}{2\pi(j-2n+k)}\cdot\sin\frac{\pi(j-2n+k)}{2}\right. \\
& + \frac{1}{2\pi(j+2n-k)}\cdot\sin\frac{\pi(j+2n-k)}{2} + \frac{1}{2\pi(j-2n-k)}\cdot\sin\frac{\pi(j-2n-k)}{2} \\
& \left. + \frac{1}{2\pi(j+2n+k)}\sin\frac{\pi(j+2n+k)}{2} + \frac{1}{\pi(j-k)}\cdot\sin\frac{\pi(j-k)}{2} + \frac{1}{\pi(j+k)}\cdot\sin\frac{\pi(j+k)}{2}\right] \\
& \times\left[\frac{3}{2}\pi\delta_{1i} + \frac{1}{2}\pi\delta_{3i}\right] - \frac{TR_m}{8}\sum_{i=1,3}\sum_{j}\sum_{n=1,3}\sum_{k} S_{ij}C_n A_k \frac{\pi^2}{l} n\cdot k \\
& \times\left[\frac{1}{\pi(j-2n+k)}\cdot\sin\frac{\pi(j-2n+k)}{2} + \frac{1}{\pi(j+2n-k)}\sin\frac{\pi(j+2n-k)}{2} - \frac{1}{\pi(j-2n-k)}\right. \\
& \left.\times\sin\frac{\pi(j-2n-k)}{2} - \frac{1}{\pi(j+2n+k)}\cdot\sin\frac{\pi(j+2n+k)}{2}\right]\left[\frac{3}{2}\pi\delta_{1i} + \frac{1}{2}\pi\delta_{3i}\right]\Bigg\} \\
& + \frac{1}{\pi(k+q)}\cdot\sin\frac{\pi(k+q)}{2} - \frac{R_o^3 - R_i^3}{4}\sum_{n=1,3}\sum_{k}\sum_{q} C_n A_k A_q \frac{\pi^4}{l^3}k^2 q^2 \\
& \times\left[\frac{1}{2\pi(2n-k+q)}\sin\frac{\pi(2n-k+q)}{2} + \frac{1}{2\pi(2n+k-q)}\sin\frac{\pi(2n+k-q)}{2} + \frac{1}{2\pi(2n-k-q)}\right. \\
& \left.\times\sin\frac{\pi(2n-k-q)}{2} + \frac{1}{2\pi(2n+k+q)}\sin\frac{\pi(2n+k-q)}{2} + \frac{1}{\pi(k-q)}\sin\frac{\pi(k-q)}{2}\right. \\
& + \pi E_0\Bigg\{\frac{R_0^4 - R_i^4}{8}\sum_{n}\sum_{q} A_k A_q \frac{\pi^4}{l^3}\cdot k^2 q^2\left[\frac{1}{\pi(k-q)}\cdot\sin\frac{\pi(k-q)}{2}\right.
\end{aligned}
$$

$$+\frac{1}{\pi(k+q)}\sin\frac{\pi(k+q)}{2}\Big]-\frac{R_o^3-R_i^3}{4}\sum_{i=1,3}\sum_{k}\sum_{q}C_nA_kA_q\frac{\pi^4}{l^3}n\cdot kq^2$$

$$\times\Big[\frac{1}{\pi(2n+k+q)}\sin\frac{\pi(2n+k+q)}{2}-\frac{1}{\pi(2n-k-q)}\sin\frac{\pi(2n-k-q)}{2}+\frac{1}{\pi(2n+k-q)}$$

$$\times\sin\frac{\pi(2n+k-q)}{2}-\frac{1}{\pi(2n-k+q)}\sin\frac{\pi(2n-k+q)}{2}\Big]+6l\cdot\left(\ln\frac{R_o}{R_i}-\frac{T}{R_m}\right)$$

$$\times\Big[\frac{1}{2}\sum_{n=1,3}C_n^2+\sum_{n=1,3}\sum_{m=1,3}C_nC_m\Big]+\Big[(R_o^4-R_i^4)-\frac{8(R_o^3-R_i^3)}{3}+4TR_m^3\Big]$$

$$\times\frac{\pi^2}{l^3}\sum_{n=1,3}C_n^2n^4+\frac{1}{3}\Big[4R_m^2\ln\frac{R_o}{R_i}-6TR_m+\frac{3(R_o^4-R_i)}{16R_m^2}\frac{\pi^2}{l}\sum_{n=1,3}C_n^2n^2\Big]\Big\}$$

δ_{ij} is the Kronecker delta, i, j, k, n, m, q are summation indices and S_{ij} are the integrated terms of $\bar{\sigma}_y$ shown in eqn (40), i.e.

$$S_{11}=-\frac{4}{\pi}1.73\sigma_y,\ S_{12}=-\frac{4}{\pi}1.1\sigma_y,\text{ etc.}$$

$$S_{2j}=-S_{ij}/3.$$

The expansion for (41) is

$$M=2\int_{R_i}^{R_o}\int_0^{\pi}\Big[r\cos\phi-\sum_{n=1,3}C_n\left(\cos\frac{2n\pi z}{l}+1\right)\cos2\phi\cos\phi$$

$$-\frac{1}{2}\sum_{n=1,3}C_n\left(\cos\frac{2n\pi z}{l}+1\right)\sin2\phi\sin\phi\Big]\Big[\sum_{i=1,3}\sum_{j}S_{ij}\cos\frac{j\pi z}{l}\cos i\phi+\frac{2}{3}E_0(2\epsilon_{zz}+\epsilon_{\phi\phi})\Big]r\,dr\,d\phi$$

which after integration gives

$$M=\frac{R_o^3-R_i^3}{3}\sum_{i=1,3}\sum_{j}S_{ij}\cos\frac{j\pi z}{l}\cdot\pi\delta_{1i}-\frac{TR_m}{2}\sum_{i=1,3}\sum_{j}\sum_{n=1,3}$$

$$\times S_{ij}C_n\cos\frac{j\pi z}{l}\left(\cos\frac{2n\pi z}{l}+1\right)\left(\frac{3}{2}\pi\delta_{1i}+\frac{1}{2}\pi\delta_{3i}\right)+\pi E_0\Big\{-\frac{R_o^4-R_i^4}{4}\cdot\sum_{k}A_k$$

$$\times\frac{k^2\pi^2}{l^2}\cdot\cos\frac{k\pi z}{l}-\frac{\pi^2(R_o^3-R_i^3)}{2l^2}\Big[\sum_{n=1,3}\sum_{k}A_kC_nn.k.\sin\frac{2n\pi z}{l}$$

$$\times\sin\frac{k\pi z}{l}-\sum_{n=1,3}\sum_{k}C_nA_kk^2\cos\frac{k\pi z}{l}\left(\cos\frac{2n\pi z}{l}+1\right)\Big]\Big\}$$

ignoring terms of the order of C_n^2 or smaller.

The work δW done by the applied couple in eqn (17) is given by $M\delta\theta$, where θ denotes the slope at the ends of the pipe shown in Fig. 5 and is given in view of Fig. 6 by:

$$\theta=\text{arc }tg\left(\frac{\partial u}{\partial z}\Big|_{z=(l/2)}\right)$$

$$=\text{arc }tg\left(\sum_{k}A_k\frac{k\pi}{l}\cdot\sin\frac{k\pi}{2}\right).$$

The above equation is replaced with the first 2 terms of the series expansion for $|\theta|<1$, rendering the work done;

$$W=M\cdot\Big\{\sum_{k}A_k\frac{k\pi}{l}\cdot\sin\frac{k\pi}{2}-\frac{1}{3}\cdot\sum_{k}\sum_{q}\sum_{p}A_kA_qA_pkqp\frac{\pi^3}{l^3}\sin\frac{k\pi}{2}\cdot\sin\frac{q\pi}{2}\cdot\sin\frac{p\pi}{2}\Big\}$$

which makes the derivative with respect to coefficients simpler. The computer program shown here is for nonlinear strain and solves for the system of equations;

$$\frac{\partial E}{\partial A_1}+\lambda_1\frac{\partial F_1}{\partial A_1}+\lambda_2\frac{\partial F_2}{\partial A_1}+\cdots+\lambda_q\frac{\partial F_q}{\partial A_1}=\frac{\partial W}{\partial A_1}$$

$$\frac{\partial E}{\partial A_2}+\lambda_1\frac{\partial F_1}{\partial A_2}+\cdots+\lambda_q\frac{\partial F_q}{\partial A_2}=\frac{\partial W}{\partial A_2}$$

$$\frac{\partial E}{\partial C_n}+\lambda_1\frac{\partial F_1}{\partial C_n}+\cdots+\lambda_q\frac{\partial F_n}{\partial C_n}=\frac{\partial W}{\partial C_n}$$

$$F_1 = BM$$

$$F_n = BM$$

where $F_1, F_2, \ldots F_q$ are the constraint equations for constant bending moment forced at q cross sections (which was 3 for this study) and $\lambda_1, \lambda_2, \ldots, \lambda_q$ are the Lagrange multipliers.